Planetary and Space Science xxx (2018) 1–14

Contents lists available at ScienceDirect

Planetary and Space Science

journal homepage: www.elsevier.com/locate/pss

Aditya Solarwind Particle EXperiment (ASPEX) onboard the Aditya-L1 mission

S.K. Goyal [a,*], P. Kumar [a], P. Janardhan [a], S.V. Vadawale [a], A. Sarkar [a], M. Shanmugam [a], K.P. Subramanian [a], B. Bapat [b], D. Chakrabarty [a], P.R. Adhyaru [a], A.R. Patel [a], S.B. Banerjee [a], Manan S. Shah [a], Neeraj K. Tiwari [a], H.L. Adalja [a], T. Ladiya [a], M.B. Dadhania [a], A. Sarda [a], A.K. Hait [c], M. Chauhan [c], R.R. Bhavsar [c]

[a] Physical Research Laboratory, Navrangpura, Ahmedabad, Gujarat, 380009, India
[b] Indian Institute of Science Education and Research, Pashan, Pune, 411008, India
[c] Space Applications Centre, Jodhpur Tekra, Ahmedabad, Gujarat, 380015, India

ARTICLE INFO

Keywords:
Sun-Earth L1 point
Aditya-L1
ASPEX
SWIS
STEPS

ABSTRACT

The Aditya Solarwind Particle EXperiment (ASPEX) is one of the seven scientific payloads onboard the Aditya-L1 mission (the forthcoming Indian solar mission), to be placed in a halo orbit around the L1 Lagrangian point of the Sun-Earth system, at a distance of 1.5 million km from the Earth, along the Sun-Earth line. ASPEX will carry out the in-situ, multi-directional measurements of the slow and fast solar wind; suprathermal particles and solar energetic particles in the energy range of 100 eV/n to 20 MeV/n. Multi-directional measurements from ASPEX will help in understanding the anisotropy in the energy distribution of particles arriving from different directions. The ASPEX payload will play a significant role in the understanding of the acceleration mechanism and generation of these energetic particles in the interplanetary medium. The ASPEX instrument has been configured as two sub-systems *viz*. the Solar Wind Ion Spectrometer and the SupraThermal & Energetic Particle Spectrometer. This paper presents the configuration details of both the sub-systems along with preliminary results obtained from the breadboard models.

1. Introduction

The solar corona, outer atmosphere of our nearest star, remains an enigma in terms of its temperature that is many orders of magnitude higher than the photospheric temperature. Closer to the surface of the Sun, the solar atmosphere is dominated by Sun's own magnetic field, which is about 10^5 nT. The plasma here is regarded as collisional with a density of about 10^8–10^9 particles per cc. However, the further we go out from the surface of the Sun, its atmosphere becomes tenuous and fluid forces start to dominate over magnetic forces. Close to the Earth's orbit at about 200 solar radii (~1 AU), the magnetic field is of the order of nanoTeslas. Plasma in this region is tenuous with a density of about ~10 particles per cc and is naturally regarded as collisionless. Clearly, different physics prevails in the lower and upper corona of the Sun. In particular, a fluid description may suffice to describe the plasma dynamics close to the surface of the Sun, but a particle description is necessary for describing the plasma at 1 AU.

As stated earlier, one of the main mysteries about the solar corona is the million-degree atmosphere above the relatively cooler (~5780 K) solar surface. Several remote sensing observations are being made from the ground as well as space to solve this puzzle. Space-borne instruments like the Transition Region and Coronal Explorer (TRACE) (Strong et al., 1994), the Solar and Heliospheric Observatory (SOHO) (Domingo et al., 1995), the Solar Dynamic Observatory (SDO) (Lemen et al., 2012) have been deployed and have contributed enormously towards understanding such issues. The Sun also emanates solar wind due to its million-degree corona (Parker, 1958; Snyder and Neugebauer, 1964) and understanding the acceleration mechanism of the solar wind is yet another major challenge in the space physics. Theory predicts that (Isenberg, 2001; Isenberg and Vasquez Bernard, 2007) wave particle interaction may play a significant role in accelerating the solar wind, but one needs in-situ observations of solar-wind particles to confirm this hypothesis.

* Corresponding author.
E-mail address: goyal@prl.res.in (S.K. Goyal).
URL: http://www.prl.res.in (S.K. Goyal).

https://doi.org/10.1016/j.pss.2018.04.008
Received 14 December 2017; Received in revised form 16 March 2018; Accepted 10 April 2018
Available online xxxx
0032-0633/

Predicting space weather accurately is also becoming important day-by-day. Solar Energetic Particles (SEP) ejected during solar flares or Coronal Mass Ejections (CME) may affect spacecraft or satellites (Feynman and Gabriel, 2000). Prediction of such SEPs rely on in-situ as well as on remote sensing observations.

Over the past three decades, a large suite of instruments onboard dedicated solar missions like the Helios 1 & 2 (Leinert et al., 1977), Ulysses (Phillips et al., 1995), WIND (Ogilvie and Desch, 1997), the Advanced Composition Explorer (ACE) (Stone et al., 1998), the Solar and Heliospheric Observatory (SOHO) etc. have contributed significantly to our understanding of the various solar wind properties such as particle flux, composition, velocity distribution etc. along with the interplanetary magnetic field (IMF). Upcoming missions like the Parker Solar Probe (Fox et al., 2016), due for launch in 2018 and the Solar Orbiter (Muller et al., 2013), due for launch in 2019 will also enhance our knowledge about the Sun and heliosphere. India's first solar mission, Aditya-L1, due for launch in 2019–2020 (Seetha and Megala, 2017) is going to contribute significantly to enhance our knowledge in solar physics by monitoring the Sun through in-situ measurements along with remote sensing observations from the L1 vantage point. Several studies in recent times (Janardhan et al., 2010; Janardhan et al., 2011; Bisoi et al., 2014; Janardhan et al., 2015a, 2015b) have shown that solar photospheric magnetic fields have been steadily declining over the past 2 decades or more along with a corresponding decline in the solar wind micro-turbulence levels. Given that Aditya-L1 is likely is be launched in 2019-2020, the expected minimum of the current solar cycle, it will be an ideal time to study particle fluxes both in and out of the ecliptic plane as the solar cycle gradually rises to its next maximum and see if more insights can be gained on the effects of the declining solar photospheric field. One of seven experiments onboard the Aditya-L1, ASPEX will constantly monitor heliospheric ions from solar wind as well as energetic phenomena such as flares, CMEs etc. (Janardhan et al., 2017). ASPEX consists of two subsystems: The Solar Wind Ion Spectrometer (SWIS) and the Supra Thermal & Energetic Particle Spectrometer (STEPS) covering an energy range of 100 eV/n to 20 MeV/n.

In the following sections, section 2 describes the overall configuration of the ASPEX payload. Details of the SWIS and STEPS subsystems are covered in sections 3 and 4 respectively while a comprehensive summary is provided in section 5.

2. Aditya Solarwind & Particle EXperiment

During the last few decades, the existence of primarily two types of solar wind (Feldman et al., 2005) has been broadly identified. One is the slow solar wind (speed ~400 km/s) in which the physical properties are highly variable and the other is the fast solar wind (speed ~700 km/s) which is much less variable. Parker's theory of solar wind (Parker, 1958) can explain the existence of the slow solar wind in the interplanetary medium. However, understanding the origin of the fast solar wind, emanating from large, cool open field regions called coronal holes remains unclear and cannot be explained by this theory. As the solar wind plasma accelerates through the heliospheric medium, its density drops off very rapidly with the radial distance from the Sun and this greatly reduces the ionization and recombination processes. Helium abundance in the solar wind is often used to determine the origin of the solar wind structure. Variations in the He^{++}/H^{+} ratio is generally steady and close to 5% in high speed streams whereas, it tends to be lower and more variable in the slow solar wind.

Solar wind plasma in the interplanetary medium is hot ($T > 10^5$ K) and poorly collisional (mean free path ~1 AU). Therefore, kinetic effects prevail in the solar wind leading to wave fluctuations that transfer energy to smaller scales through a cascading process. As the Coulomb collisions become secondary and wave particle interactions become dominant, heating of the particles begins to take place. This process is believed to play an important role in the generation of the suprathermal or non-Maxwellian particle population in the solar wind, although the exact generation processes are still not clear. Therefore, the distribution of charged particles in the solar wind comprises of two distinctly different components. The low energy thermal particles and a suprathermal halo component are believed to be isotropically distributed at all pitch angles, although detailed investigations in this regard are extremely sparse. Suprathermal ions (e.g. H^{+}, He^{++} etc.) are distinctively present in the solar wind (Chotoo et al., 2000). In the fast solar wind, the suprathermal electrons consist of a magnetic field-aligned strahl population, which is highly energetic and usually moves in the anti sunward direction. In addition to the suprathermal ions, there are other important sources of energetic ions close to 1 AU with energies ranging from less than 100 keV to several tens of MeVs. These energetic ions can be generated, during solar flares or coronal shock events (e.g. SEPs) or by the interplanetary (IP) shocks driven by Interplanetary CMEs (ICMEs), co-rotating interaction regions (CIRs) or in many cases, possibly by the Earth's bow shock.

The primary focus of the ASPEX payload on-board the ADITYA-L1 satellite is to understand the solar and interplanetary processes (like shock effects, wave-particle interactions etc.) in the acceleration and energization of solar wind particles. In order to achieve this, it is necessary that ASPEX measures low as well as high energy particles that are associated with both the slow and fast components of solar wind, suprathermal population, shocks associated with CME and CIR and SEPs. Among these, it is expected that the slow and fast components of the solar wind and some part of the suprathermal population can be measured in a predominantly radial direction. In addition, a part of the suprathermal population, CME and CIR-accelerated particles and SEPs are expected to arrive at the detectors along the Parker spiral.

It is known that He^{++}/H^{+} ratio is an important proxy that can be used to determine the arrival of a CME driven shock front at 1 AU (Steiger and von Richardson, 2006). ASPEX will use the He^{++}/H^{+} ratio as a compositional "flag" to differentiate (and identify) the arrivals of CME, CIR, SEP-related particles from those of the quiet solar wind origin. Therefore, it is necessary that the measurements are planned suitably so that all the science objectives are fulfilled. The major science objectives of the ASPEX payload are as follow:

- Can we get insights into the generation mechanism(s) of suprathermal and other energetic ions in the interplanetary space?
- How are these ions associated with the solar processes?
- Can the particles associated with interplanetary shock processes (associated with CME, CIR etc.) be identified and the shock related processes be addressed?
- Does anisotropy in the energy distribution of particles exist in the direction of the Parker spiral vis-à-vis other directions?
- How does the He^{++}/H^{+} number density ratio change corresponding to various solar events (Flares, CME's, CIR's) and what is the range of values for this ratio?
- What is physical mechanism responsible for the increase in the He^{++}/H^{+} number density ratio?
- What is the importance of the above-mentioned processes for the impact on the near-earth space weather?

Addressing the above mentioned issues require systematic observations of particle fluxes at selected energy ranges as well as measurements of the He^{++}/H^{+} number density ratio at the L1 Lagrangian point. Keeping this in mind, the ASPEX payload has been configured as two independent subsystems. The SWIS subsystem consisting of two independent units will have the capability of measuring solar wind particles in the energy range of 100 eV to 20 keV in the plane of the ecliptic and normal to the plane of the ecliptic, using an electrostatic analyzer (ESA) coupled to a micro channel plate (MCP) detector. While one of the SWIS units, referred to as Top Hat 1 (THA-1) will receive and differentiate particles (H^{+} and He^{++} ions) in the ecliptic plane (species differentiation mode), the second SWIS unit, referred to as Top Hat 2 (THA-2) will measure the total flux irrespective of types of species across the ecliptic plane (species integrated mode). The STEPS subsystem will measure the particle flux in the 20

keV/n to 20 MeV/n energy range in the Sunward, anti-Sunward, Parker, ecliptic North and ecliptic South directions, using custom designed silicon detectors. Three STEPS units (Sunward, Parker and anti-Sunward) are designed to operate in the species differentiation mode while the remaining three STEPS units (between Sunward and Parker, ecliptic North and ecliptic South) will operate in the species-integrated mode (Goyal et al., 2016).

The directional details of the THA-1, THA-2 of the SWIS and their capability for the separation of the He^{++} and H^{+} particles are covered in section 3. The details of the STEPS-1 package, STEPS-2 package, their detector units, directional information and capability of separation of the species are covered in section 4. Table 1 provides details of the various packages of the ASPEX payload.

3. Solar Wind & Ion Spectrometer

The SWIS subsystem is a low energy ion spectrometer operating in the energy range of 100 eV-20 keV. This energy range of the SWIS instrument will measure the mass, energy and direction of the fast and slow components of solar wind particles. Table 2 provides the details of the scientific, observation and instrument requirements for the SWIS.

3.1. SWIS configuration

The SWIS instrument is configured to have two units having FOVs in the ecliptic plane and perpendicular to it. It comprises of two top-hat analyzers, THA-1 and THA-2 each having an FOV of 2π along the analyzer azimuthal plane and ±2deg along the analyzer elevation plane. The analyzer unit having FOV along the ecliptic plane (THA-1) comprises of a hemispherical energy analyzer and a magnetic mass analyzer (MMA). The other SWIS unit, THA-2 having an FOV perpendicular to the plane of ecliptic does not contain the MMA. The ESA scans the energy of the incoming particles in the instrument FOV. The MMA deflects incident ions based on the Lorentz force. The geometry of the incident ions and the magnetic field pattern inside the MMA results in radial deflection of the particles on the detector plane. These ions are detected by an MCP (chevron stack) followed by a position sensitive detector which gives the information on mass and direction of the incident particle. The instrument details are presented in Table 3.

3.2. ESA design and configuration

The electrostatic analyzers used in both the THA-1 and THA-2 consist of two concentric hemispheres with a radial field inside the channel. The incoming particle is energy scanned using an appropriate field inside this channel. Simulations using the SIMION software (Simion, 2008) were performed to understand the performance of the ESA and to finalize an optimized geometry of the analyzer. The model used for the study of the ESA section using SIMION is shown in Fig. 1.

The geometric factor of the SWIS instrument was also determined from these simulations. A focusing grid assembly to focus the ion beam just after the ESA section was designed and the beam footprint on the detector was also characterized based on these simulations.

Table 2
SWIS scientific, observation and instrument requirements.

Scientific Requirement	Observation Requirement	Instrument Requirement
Continuous in-situ measurement of solar wind particles	Measure energy spectrum of protons, alpha and heavier particles in energy range of 100 eV to 20 keV	Electrostatic energy analyzer combined with a magnetic mass analyzer
Study of angular distribution of solar wind particles to understand origin of supra-thermal ions	Measure energy and mass spectrum of solar wind particles in and across the ecliptic plane	2π Field of View (FOV) each in and across ecliptic plane and position sensitive detection
Investigate energy dependence of alpha (He^{++})/proton (H^{+}) ratio	Measure proton and alpha particle flux at different energy	Mass separator with sufficient resolution to separate alpha and proton in the desired energy range
To investigate the temperature anisotropy of solar wind particles	Measure velocity components of particles in direction parallel and perpendicular to the inter-planetary magnetic field	2π FOV each in and across ecliptic plane and position sensitive detection

Table 3
SWIS instrument details.

Parameters	Values
Sensor units	Two (THA-1: FOV in the ecliptic plane and with MMA, THA-2: FOV in the plane perpendicular to ecliptic without MMA)
Energy range	100 eV to 20 keV
Energy Resolution (ΔE/E)	10% for both THA-1 and THA-2
Analyser constant	18 for both THA-1 and THA-2
FOV	2π for both the sensors
Detector	80 mm Chevron MCP with position sensitive anode for both sensors
Magnets	16 Sm-Co magnets to be used in THA-1

3.3. Magnetic Mass Analyzer

Energy selected ions from the ESA section are subjected to mass differentiation using the MMA which consists of 16 thin Sm-Co permanent magnets arranged in a circular fashion. This constitutes a circular magnetic field inside the MMA region which deflects incident particles radially inwards with a force proportional to the mass of the particles. The field inside this region was characterized using MATLAB (Matlab, 2016). The typical field pattern at Z = 0 plane is shown in Fig. 2.

3.4. Resistive Anode Encoder

The in-house development of a position sensitive detector based on the concept of charge division was undertaken for this instrument. Since the instrument primarily looks for proton and alpha particles, a simple

Table 1
Overall specifications of the ASPEX instrument.

		SWIS	STEPS
Energy range		100 eV to 20 keV	20 keV/n to 20 MeV/n
Detectors		ESA + MCP	Silicon detectors and Scintillators
Front End Electronics (FEE)/High Voltage (HV) package	Total packages	Four	Two
	Weight	1.5 kg (THA-1) + 0.75 kg (THA-2) + 0.6 kg (THA-1-FEE) + 1.15 kg (HV unit)	2 kg (STEPS-1) + 1 kg (STEPS-2)
Processing electronics (PE)	Total packages	One (common for SWIS & STEPS)	
	Weight	3 kg (FPGA based PE)	
	Harness + local potting	1 kg	
SWIS elevated structure		1.6 kg	
Total weight		12.6 kg	
Total raw power		~35 W	

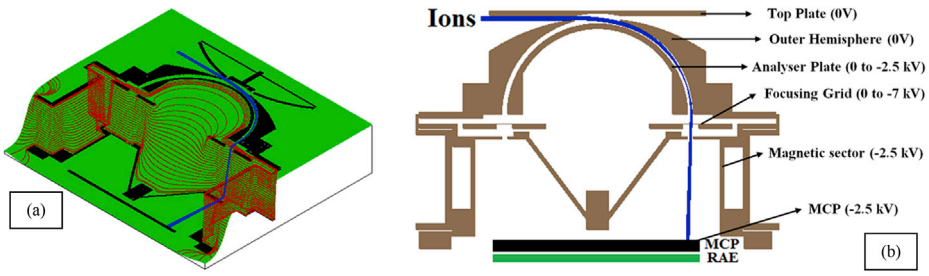

Fig. 1. (a) Potential energy view in SIMION of THA-1, (b) Various potential arrays used in the simulation with bias voltages applied to different electrodes.

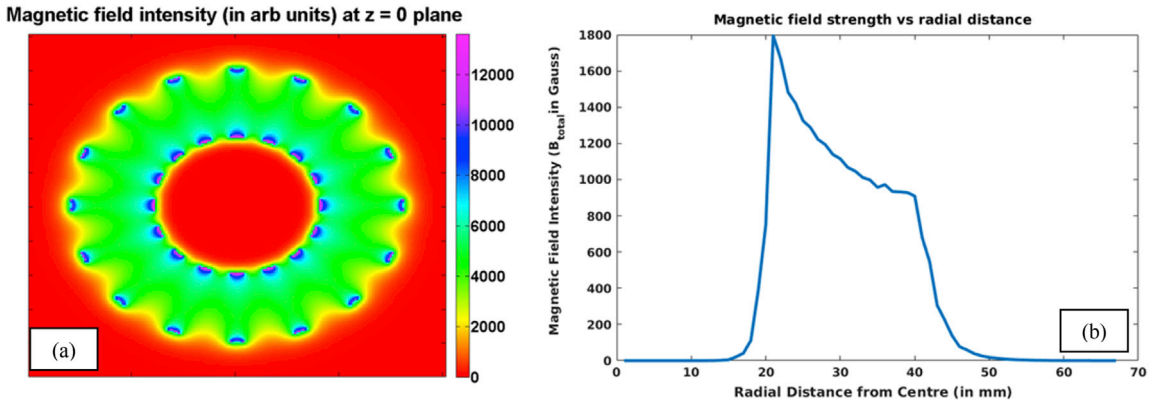

Fig. 2. (a) Magnetic field pattern inside MMA region due to circular arrangement of 16 permanent magnets, (b) Magnetic field variation as a function of radial distance.

yet robust scheme for position determination was worked out. The position information is obtained using a resistive anode encoder (RAE), which consists of multiple metallic tracks printed on a PCB material. Each of the tracks is in turn connected through known resistances resulting in a resistive chain, which is readout across its two ends. The charge collected by the front-end electronics from the two readouts of a resistive chain in turn depends on the position of the incident particle. In THA-1, the RAE consists of 4 such resistive chains consisting of 114 equally spaced tracks. Each resistive chain has four sectors resulting in an angular resolution of 22.5°. In THA-2, since the MMA is not present, the footprints of the particles on the detector are limited to an annular region around the mean radius of the ESA. Accordingly, the RAE in THA-2 consists of thin annular strip of a single resistive chain having 16 sectors resulting in an angular resolution of 22.5°. Schematic representations of the RAEs used in both the analyzers are shown in Fig. 3.

The laboratory models for both THA-1 and THA-2 have been designed and the CAD models are shown in Fig. 4.

3.5. Block schematic of the SWIS electronics

The charge collected across each resistive chain in both RAEs is processed by respective FEE channels. The output charge from the RAE is converted into voltage pulse using the charge sensitive preamplifier (CSPA) followed by the pulse shaping amplifier. The output of the

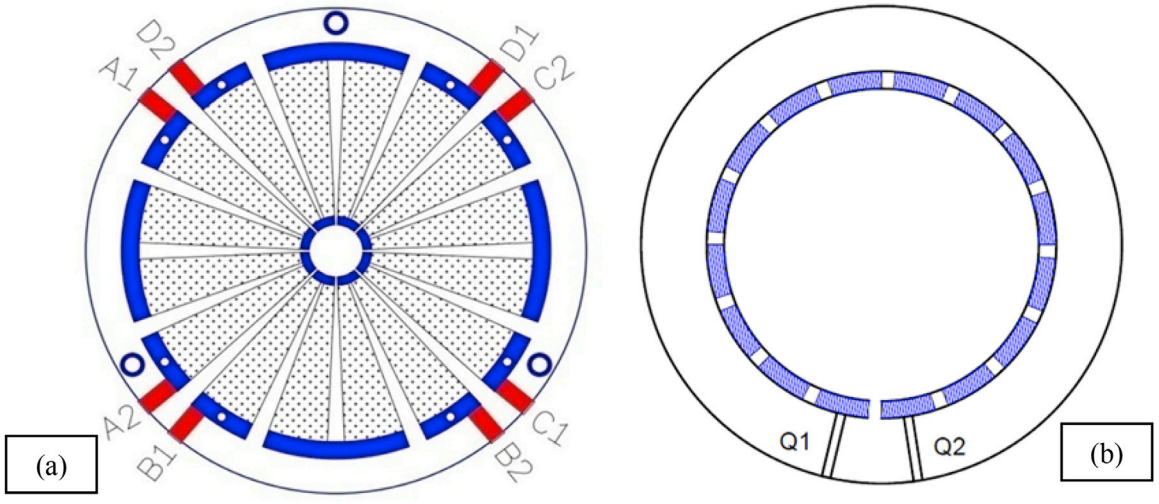

Fig. 3. Schematic representation of the resistive anode encoder employed in SWIS: (a) RAE used in THA-1 having one pair of readout per quadrant and (b) RAE used in THA-2.

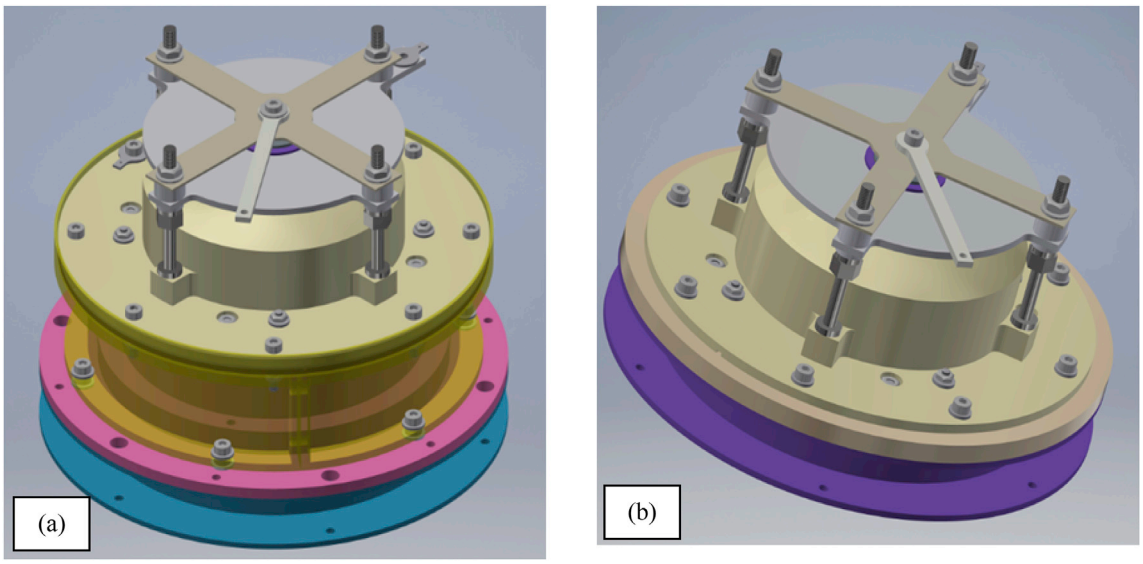

Fig. 4. CAD models of the top hat analysers: (a) THA-1 with MMA, (b) THA-2.

shaping amplifier is the Gaussian shape pulse in which the peak amplitude is proportional to the amount of the charge detected. The peak detector detects the peak, which is further digitized using analog to digital converter (ADC) to the digital numbers. The processing electronics processes these pulses to generate the position histogram as per the following equation (Leo, 1994).

$$x = \frac{V2}{V1 + V2} \times Length\ of\ resistive\ channel$$

V1 and V2 are the voltages detected at both the ends of the track. Processing electronics also controls the ADCs, the peak detectors and the high voltage supplies. The block schematic of the SWIS instrument is shown in Fig. 5.

3.6. Lab experiments

Laboratory experiments have been carried out using THA-1 along

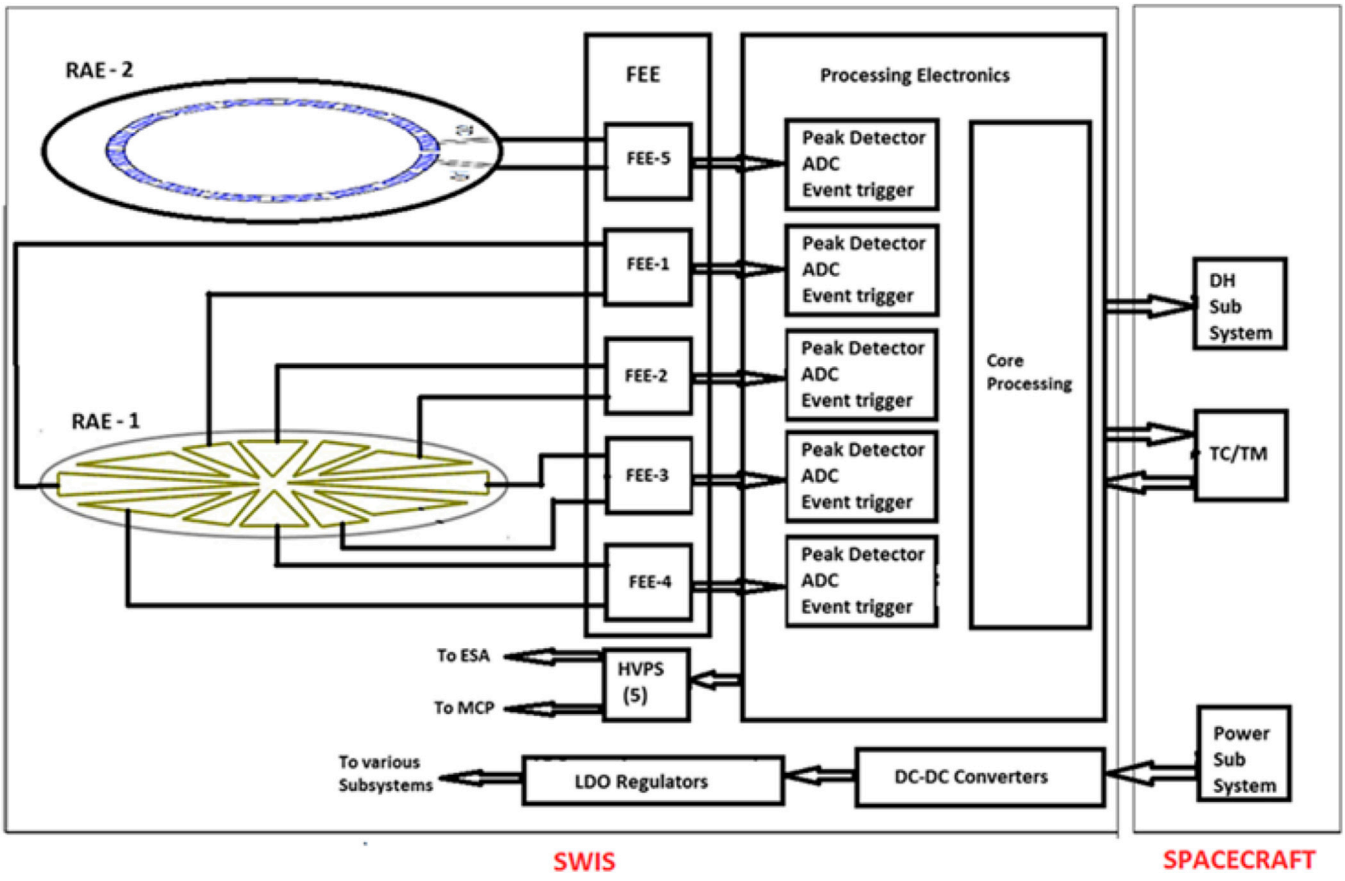

Fig. 5. Block schematic of the SWIS electronics.

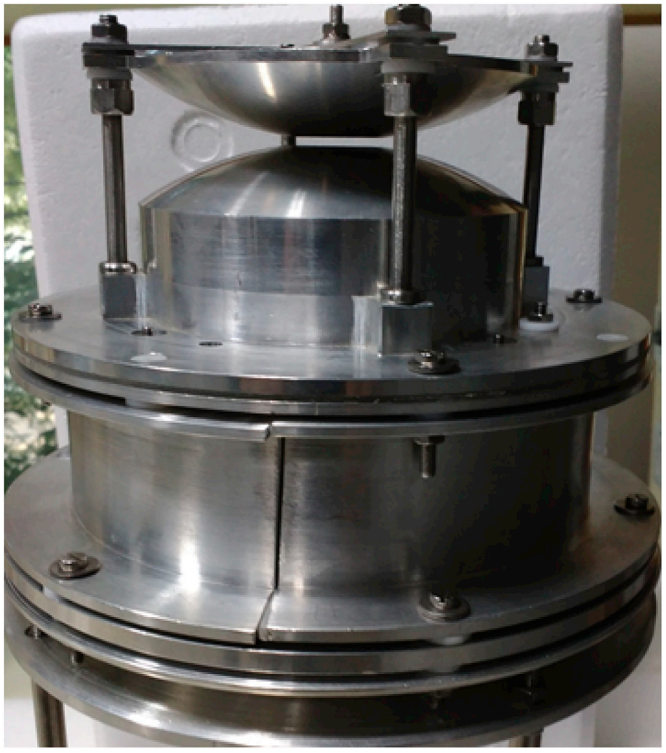

Fig. 6. Lab model of the THA-1.

with MMA as shown in Fig. 6. A Nier-type ion gun was used as an ion source for these experiments. The THA-1 was mounted on a rotating flange so as to cover each sector of the RAE.

The energy response of the ESA and mass deflection by the MMA were measured in these experiments. The results for the same are shown in the Fig. 7. The energy resolution obtained with the simulation matches well with the experimental results. The magnetic deflection values were also obtained at different energies for both proton and alpha particles and are shown in Fig. 7. Based on these experiments and ion trajectory simulations for the ESA and MMA, engineering model (EM) design of these analysers is in progress. The performance of the designed FEE for the experiments conducted on the lab model is satisfactory and the engineering model design for the same is under progress.

4. SupraThermal & Energetic Particle Spectrometer

The scientific objective of STEPS is to investigate the origin of the suprathermal particles and their relationship with the primary solar wind constituents. This will be addressed by measuring the spectrum of H^+ and He^{++} particles from multiple directions in the energy range 20 keV/n to 20 MeV/n with a relatively narrow conical field of view. Table 4 provides the details on the scientific, observation and the instrument requirements for the STEPS.

Table 4
STEPS scientific, observation and instrument requirements.

Scientific requirement	Observation requirement	Instrument requirement
Study of suprathermal particles as well as SEP ions	Measure energy spectrum of He^{++}, H^+ in the energy range of 20 keV to 20 MeV/n	Solid state detector (magnetically deflect electrons)
Study of angular distribution of suprathermal and high energy particles	Measure energy spectrum from multiple directions	Narrow conical FOV, six independent units of STEPS
Investigate energy dependence of He^{++}/H^+	Measure energy spectrum of He^{++} and H^+ separately	Two detectors in each unit of STEPS. Each detector with different dead-layer thickness
Attempt to investigate the temperature anisotropy of solar wind particles	Measure velocity components of particles in direction parallel and perpendicular to the interplanetary magnetic field	One STEPS viewing the general direction of Parker's spiral magnetic field. Other units viewing local zenith and nadir directions

4.1. STEPS configuration

The accommodation of 6 viewing directions on a single package of the STEPS subsystem is not possible. Hence, STEPS has been configured into two different packages *viz.* STEPS-1 & STEPS-2. The STEPS-1 package will be mounted on the Aditya-L1 spacecraft in the Sun viewing direction, while the STEPS-2 package will be mounted in the anti-Sun direction of the spacecraft. The CAD models of the STEPS packages are shown in Fig. 8.

The STEPS-1 package has four detector units and a stack of 3 PCBs for the FEE while the STEPS-2 package has two detector units and a stack of 3 PCBs for the FEE. The rectangular shaped detector unit (two units in STEPS-1 and one unit in STEPS-2) provides species differentiated energy spectra and uses a custom designed Si-PIN detector and a scintillation detector for the measurement of the energy and the type of incident particle. The circularly shaped detector unit (two units in STEPS-1 and one unit in STEPS-2) uses a single window Si-PIN detector for the integrated energy spectra. Table 5 provides the details for the FOVs and pointing directions of all detector units.

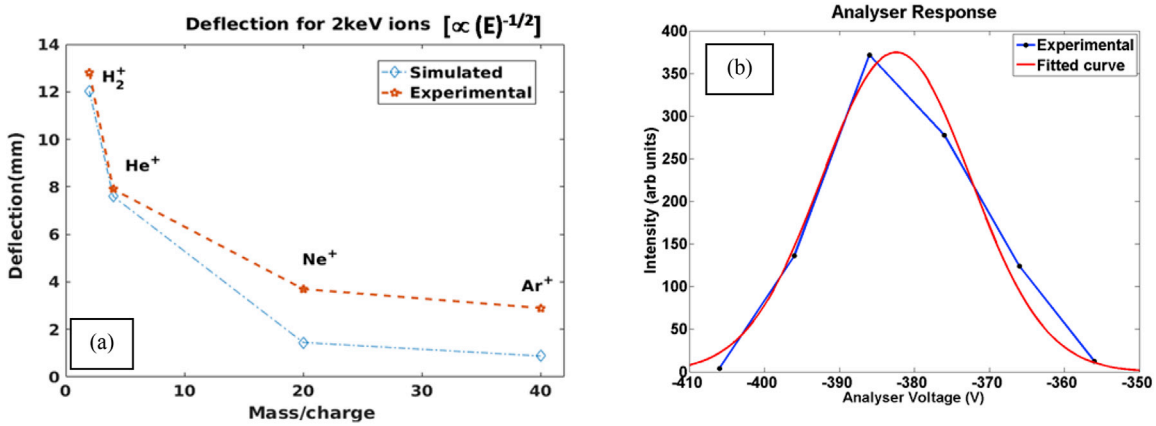

Fig. 7. (a) Typical values of radial deflection obtained for different ions using lab model of THA-1, (b) Energy analyser response of the ESA at one set value of energy and fixed beam to instrument aperture angle.

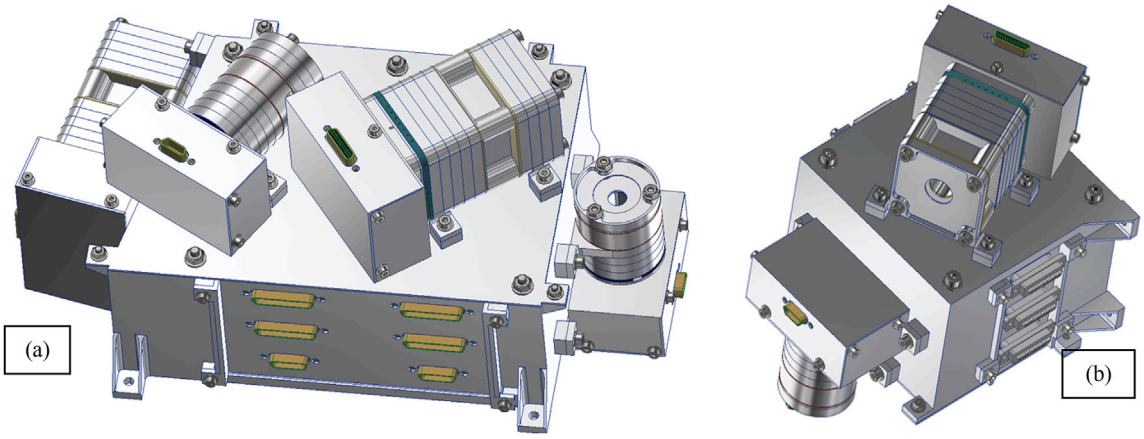

Fig. 8. (a) STEPS-1 package, (b) STEPS-2 package.

Table 5
FOV and pointing direction of each detector unit.

Type	Direction	FOV axis	FOV
Species separated spectra (rectangular detector units)	Sunward Radial (SR)	12° W of Sun-spacecraft line, in ecliptic plane	±10.5°
	Parker Spiral (PS)	52.5° W of Sun-spacecraft line, in ecliptic plane	±15°
	Earth Pointing (EP)	24° W of Earth-spacecraft line, in ecliptic plane	±18.5°
Species integrated spectra (Circular detector units)	Intermediate, between Sun and Parker spiral (IM)	30° W of Sun-spacecraft line, in ecliptic plane	±7.5°
	North Pointing (NP)	Perpendicular to ecliptic plane, towards north	±14°
	South Pointing (SP)	Perpendicular to ecliptic plane, towards south	±14°

4.2. Detector configuration for species separated spectra unit

The STEPS subsystem will measure proton and alpha particles separately for energies > 20 keV. However, it is not possible to achieve this low energy threshold using either a single silicon detector or with the ΔE-E configuration because these particles get absorbed within top few microns of the detector. To get the separation of the protons and alpha particles, we are using two detectors on a common silicon substrate, with each detector having a different entrance window thickness of high Z material.

The schematic arrangement shown in Fig. 9 (a) is for particle type identification in ΔE-E configuration. A permanent magnet assembly with SmCo magnets and Mu metal shielding is used for deflecting electrons. The dual window detector shown in Fig. 9 (b) is a custom designed Si-PIN detector from Micron semiconductor, UK. The inner section of the detector is 9 mm in diameter while the outer section of the detector extends in an annular strip from 9 mm to 18 mm. The inner detector has a very thin dead-layer window with a thickness of ~0.1 μm, which allows both protons and alpha particles of energy >20 keV to pass through while only slightly modifying their energy spectra. The outer detector has a thicker dead-layer window with a thickness of ~1 μm, which blocks alpha particles up to an energy of ~1 MeV but allows protons of the energy >150 keV as shown in Fig. 10. The lower cutoff energy of protons and alpha particles is dependent on the window thickness (0.1 μm, 1.0 μm) while the higher energy cutoff is dependent on the thickness of the silicon detector (300 μm). A plastic scintillation detector is placed below the silicon detector so that high energy particles (protons > 6 MeV) deposit a fraction of their energy in the silicon detector and then rest of their energy is deposited in the plastic scintillator. The readout of the plastic scintillator detector is done using an array of Silicon Photomultipliers (SiPMs), mounted on one of the sides of the scintillator (Fig. 9 (c)).

The CAD model of the species separated spectra unit is shown in Fig. 11. There are total 3 of such units labeled as Sunward Radial (SR), Parker Spiral (PS) and Earth Pointing (EP) in STEPS. The number of collimators used in the each detector unit is as per the FOV requirements which also affects the electron cutoff energy. The CSPA PCB for all 3 detectors (Inner detector of Si-PIN, outer detector of Si-PIN and SiPM) is placed in each detector unit to achieve better signal to noise ratio.

4.3. Design of magnetic assembly for species separated spectra unit

The solar wind contains protons, alpha, electrons and other heavier particles. The flux of electrons is much more variable than other types of particles. The solid-state detectors are also sensitive to the electron interactions and thus this interferes with the energy of the protons and other heavier particles being measured. In fact, during episodes of very large electron flux, the silicon detector can get fully saturated due to these electron interactions. To avoid this, a magnetic assembly using permanent magnets is used in each detector unit to completely deflect the electrons up to a certain energy. This is a well proven technique and is used in most of the instruments which are sensitive in this energy range. Fig. 12 (a) shows the CAD model design of the magnetic assembly using two SmCo magnets of size $24 \times 3 \times 10\ mm^3$. The magnetic field is aligned to be across the 3 mm thick section of the magnet. The Mu metal used for shielding is 3 mm thick. Fig. 12 (b) (c) & (d) show a simulation of the magnetic fields obtained using COMSOL software (Comsol Inc.). The magnetic field leakage outside the magnetic assembly is ~100 nT at a distance of 12 cm. Using this design, electrons up to the energy of 2 MeV are deflected and they do not reach to the Si-PIN detector.

4.4. Detector configuration for species integrated spectra unit

There are three detector units for the species integrated energy spectra labeled as Intermediate (IM), North Pointing (NP) and South Pointing (SP). Two of these units (IM and NP) are in the STEPS-1 package while the SP unit is in the STEPS-2 package. These detector units measure the energy spectra without particle identification. Fig. 13 (a) shows the Si-PIN detector and Fig. 13 (b) is the CAD model design of the species integrated energy spectra unit. The single window Si-PIN detector has been procured from the Micron semiconductor, UK. The active area diameter is 8 mm, made on a substrate having an area of $10.2 \times 10.2\ mm^2$ on a circular PCB of 36 mm in diameter. The number of collimators in each detector unit is decided based upon the FOV

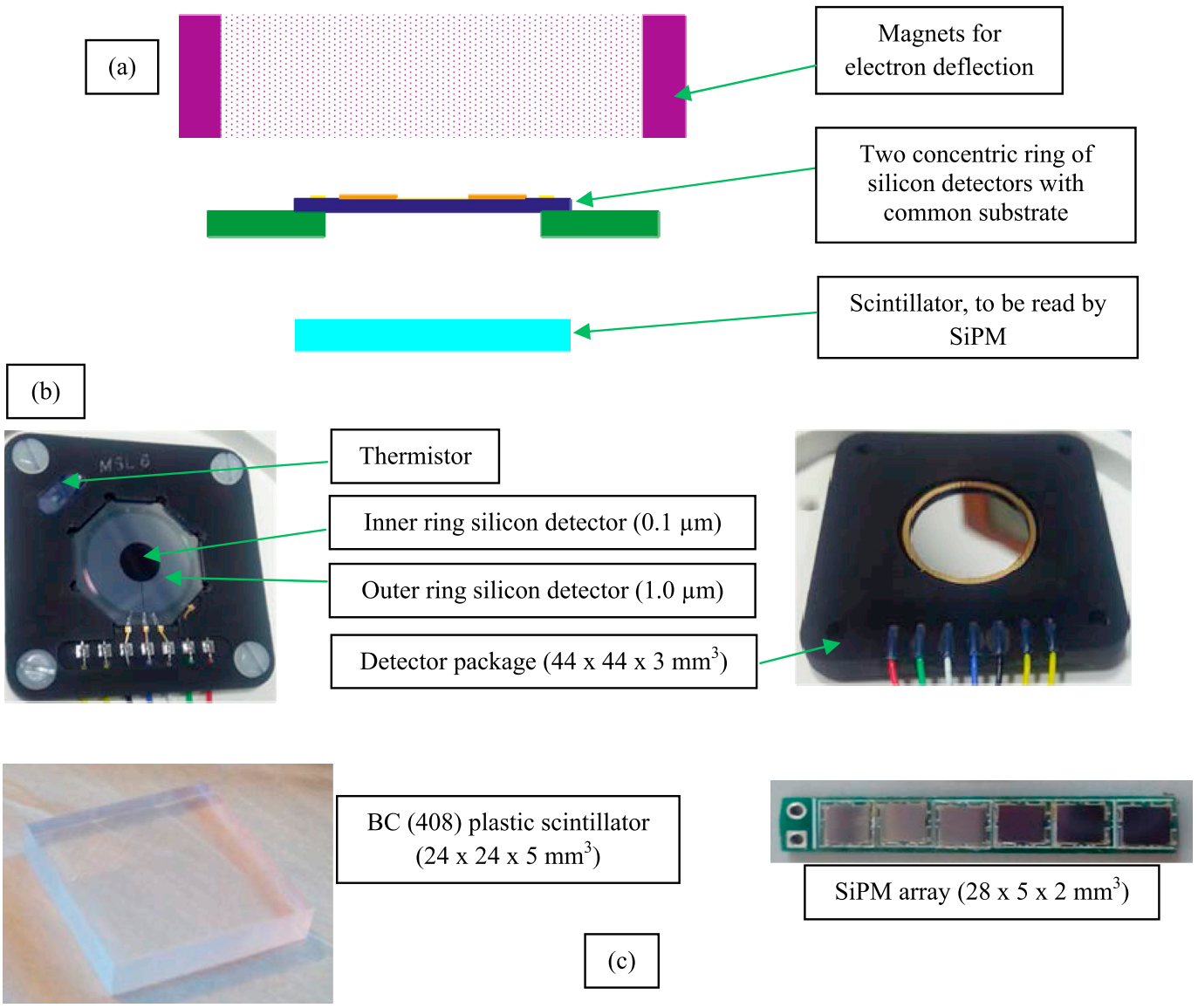

Fig. 9. (a) Detector configuration for particle identification, (b) dual window Si-PIN detector – top view & rear view, (c) plastic scintillator & SiPM array.

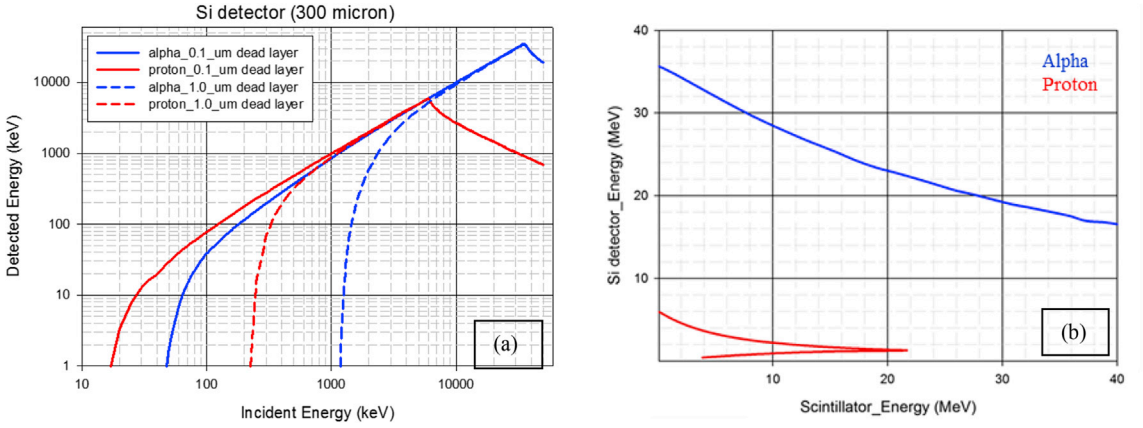

Fig. 10. (a) GEANT4 simulation for Silicon detector having two different thicknesses of entrance window, (b) GEANT4 simulation for the Energy deposited in Si detector and Scintillation detector (Agostinelli et al., 2003). (For interpretation of the references to colour in this figure legend, the reader is referred to the Web version of this article.)

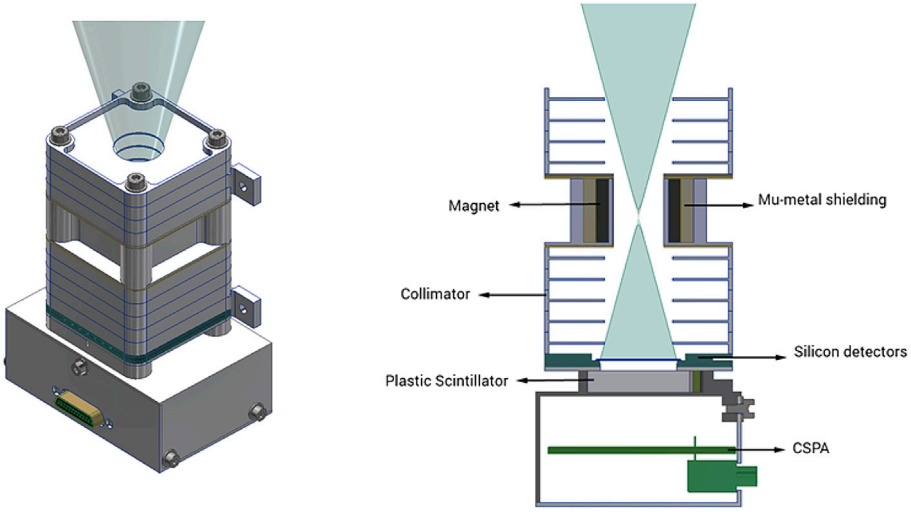

Fig. 11. CAD model of the detector unit for species separated spectra.

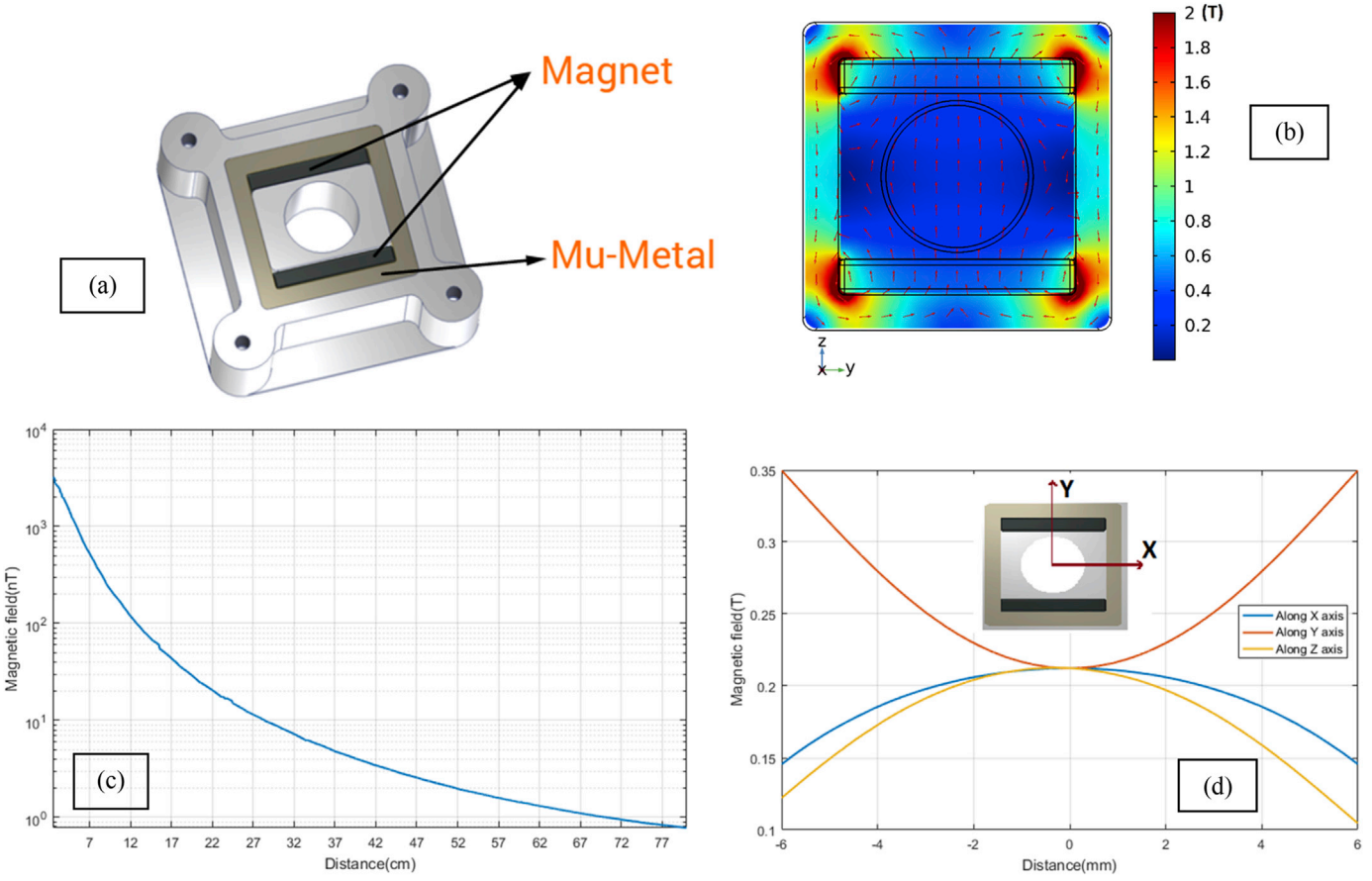

Fig. 12. (a) CAD model of the magnetic assembly for species separated spectra unit, (b) COMSOL simulation of the magnetic field, (c) magnetic field leakage outside the magnetic assembly, (d) magnetic field inside the assembly.

requirements which also affects the cutoff energy for the electron deflection.

4.5. Design of magnetic assembly for species integrated spectra unit

The species integrated spectra unit consists of a magnetic assembly designed using SmCo permanent magnets and Mu metal shielding. Fig. 14 (a) shows the CAD model design of the magnetic assembly.

The size of the SmCo magnet is $12 \times 2 \times 10\ mm^3$. The magnetic field is aligned across the 2 mm thick section of the magnet. The Mu metal shield is 2 mm thick. The magnetic simulation using COMSOL multi-physics software is shown in Fig. 14 (b) (c) & (d). The magnetic field leakage outside the assembly is ~100 nT at a distance of 10 cm. Electrons up to the energy of 1.4 MeV are deflected and they do not reach to the Si-PIN detector.

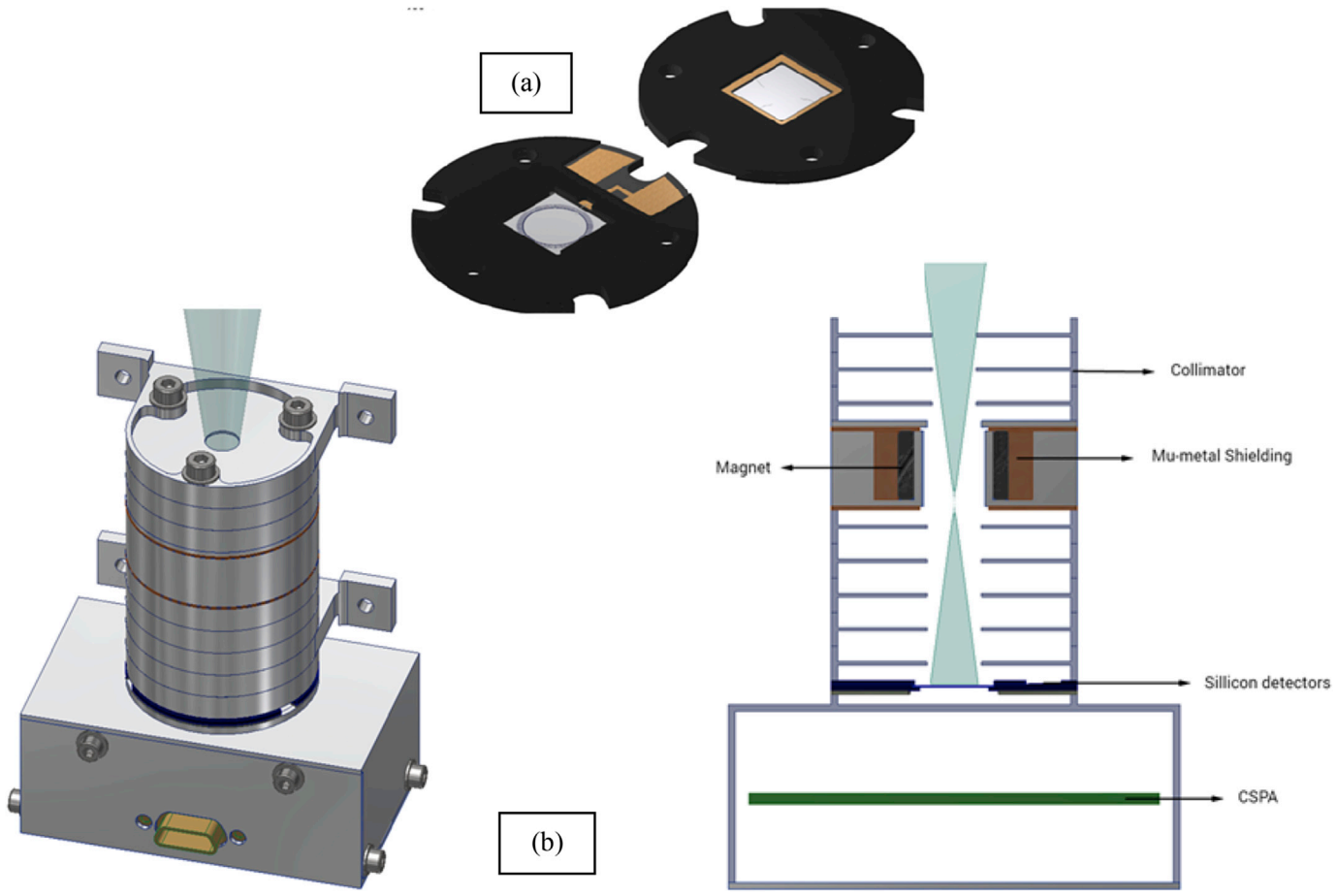

Fig. 13. (a) Single window Si-PIN detector – top and rear view, (b) CAD model design of the species integrated spectra unit.

4.6. Block schematic of the STEPS electronics

As discussed in the earlier subsections, there are total 6 detector units in the STEPS with three units having particle identification capability and other three units for integrated energy spectra. Si-PIN detectors are operated in the reverse bias mode, where particle interaction takes place in the depletion region. The amount of output charge from the detector is linearly proportional to the deposited energy. The scintillator detector gives visible light photon output after the interaction of the particle with the scintillation material. The number of the output photons is linearly proportional to the amount of the energy deposited. SiPM is a new device, used for the detection of the photons. In STEPS, the output photons from from the scintillator are read using SiPMs. The advantages of SiPM over conventional photo multiplier tube are: its compactness, low biasing voltage requirement and insensitivity to the magnetic field. The block schematic of the STEPS readout system is shown in Fig. 15.

Three independent FEE chains are essential to acquire the signal from the dual window Si-PIN detector and the plastic scintillator for the particle identification. For integrated energy spectrum, only one FEE chain is used. The readout chain consists of a CSPA for charge to voltage conversion followed by a shaping amplifier, which provides the necessary gain with Gaussian pulse shaping for improved signal to noise ratio. The shaping amplifier is designed with two gain chains to cover the energy range of 20 keV/n to 20 MeV/n. The output of the shaping amplifier is interfaced to an FPGA based processing and control system to hold the peak signal amplitude, using peak-hold detector and then converted to digital numbers using ADC. The same readout technique is adapted for all the detectors. The total energy of the incoming particle is calculated based on the energy deposited in the silicon detector and the plastic scintillator.

4.7. Experimental setup and results for dual window Si-PIN detector and scintillator detector

The dual window Si-PIN detector has been tested with X-ray sources (^{241}Am & ^{109}Cd). Fig. 16 (a) shows the dual window detector with the FEE. The detector is biased to +60 Vdc and its output is AC coupled to the CSPA. The CSPA is designed using 2N4416 FET and LM6172 op-amp. The CSPA output is further amplified using pulse shaping amplifier with pulse peaking time of 3 μs. The shaping amplifier output is acquired using multi-channel analyzer. Fig. 16 (b) shows the setup where both the inner window detector and the outer window detector are read simultaneously. Fig. 16 (c) shows the spectrum output, acquired for 1800s. It is seen from the figure that the desired energy threshold of ~10 keV can be achieved with this detector, which is essential for the STEPS. The testing of the setup was carried out in a light tight box to minimize the noise due to external light.

Fig. 17 (a) shows the plastic scintillator and SiPM array PCB. The SiPM PCB is mounted on one of the sides of the plastic scintillator. The assembly is wrapped with the aluminum foil, for the internal light reflection and to avoid any stray light leakage. The assembly is further covered with black paper to ensure that it is light tight. The BC408 plastic scintillator has been procured from M/s Saint Gobain crystals and the SiPM (MicroC series SiPM) has been procured from the SensL. The SiPM is biased to +27 Vdc. The output of the SiPM is AC coupled to the RC feedback type CSPA. LM6172 op-amp is used for both CSPA and shaping amplifier. The shaping amplifier peaking time is set to 0.3 μs. Fig. 17 (b) shows the output of the setup. The result shows that 22 keV energy line from the ^{109}Cd radioactive source can be detected.

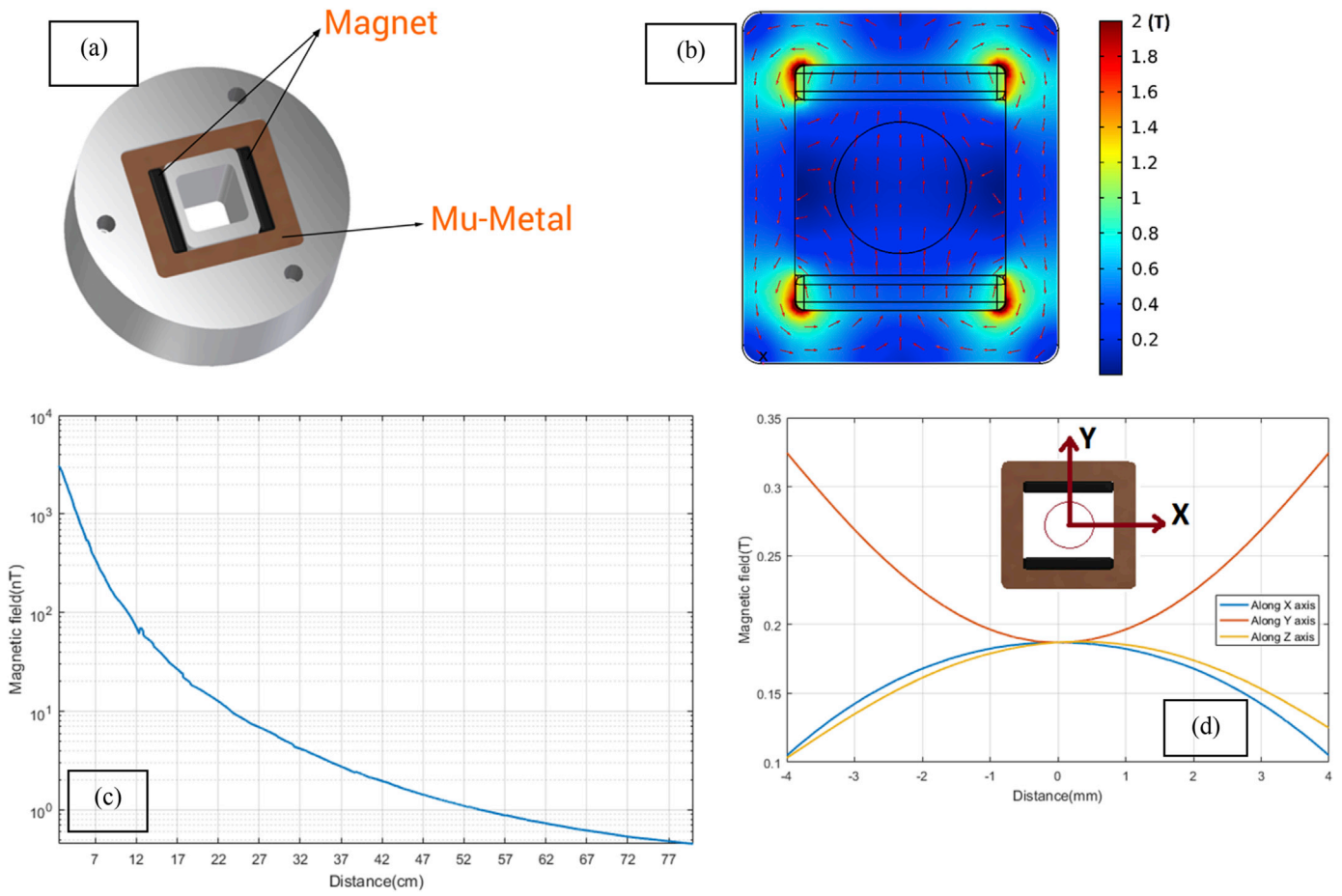

Fig. 14. (a) CAD model of the magnetic assembly for species integrated spectra unit, (b) COMSOL simulation of the magnetic field, (c) magnetic field leakage outside the magnetic assembly, (d) magnetic field inside the assembly.

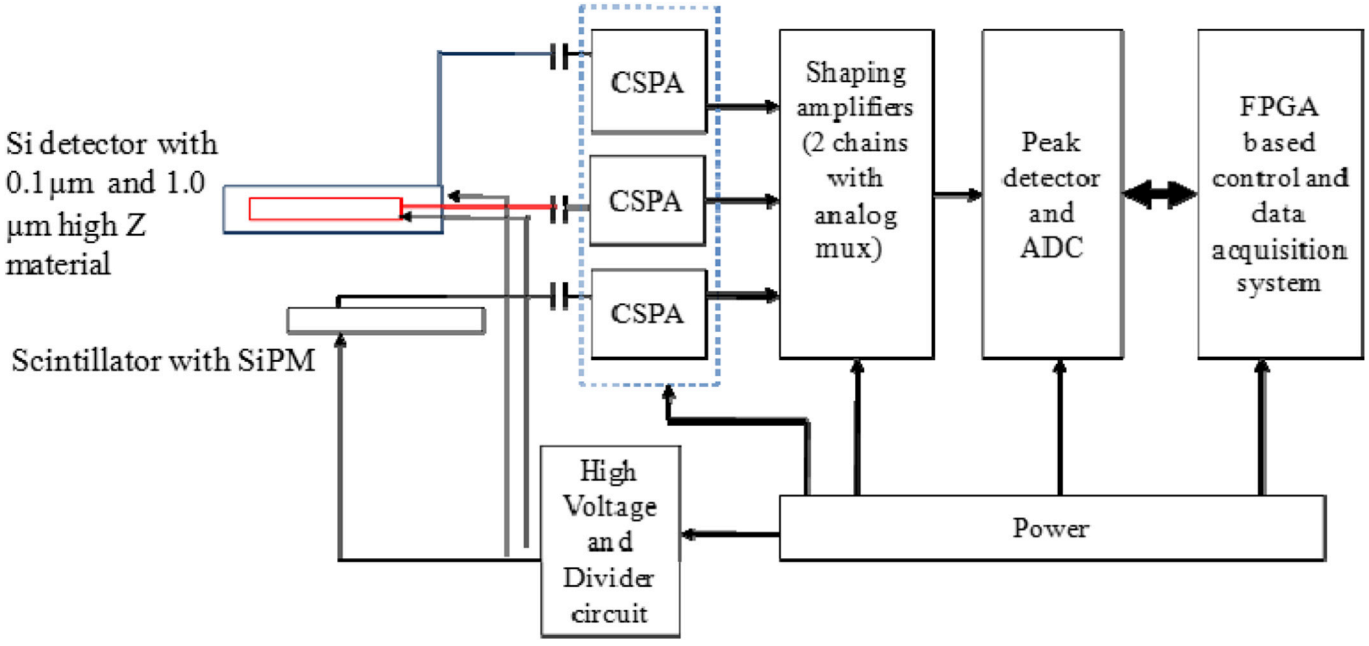

Fig. 15. Block diagram of the electronics for the species separated spectra unit.

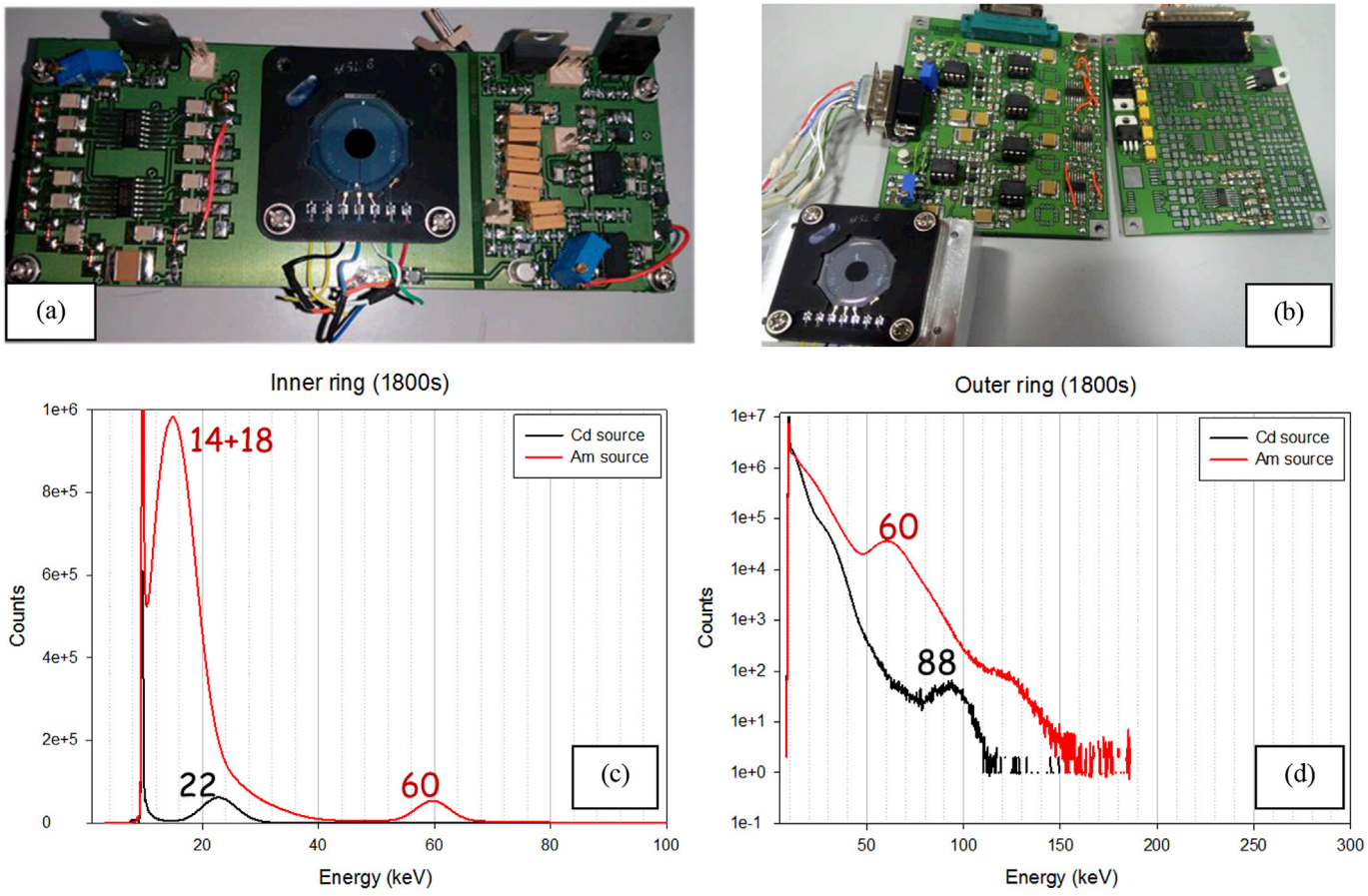

Fig. 16. (a) Dual window Si-PIN detector with single chain FEE, (b) Dual window Si-PIN detector with double chains of FEE, (c) Energy spectrum for inner window detector, (d) Energy spectrum for outer window detector.

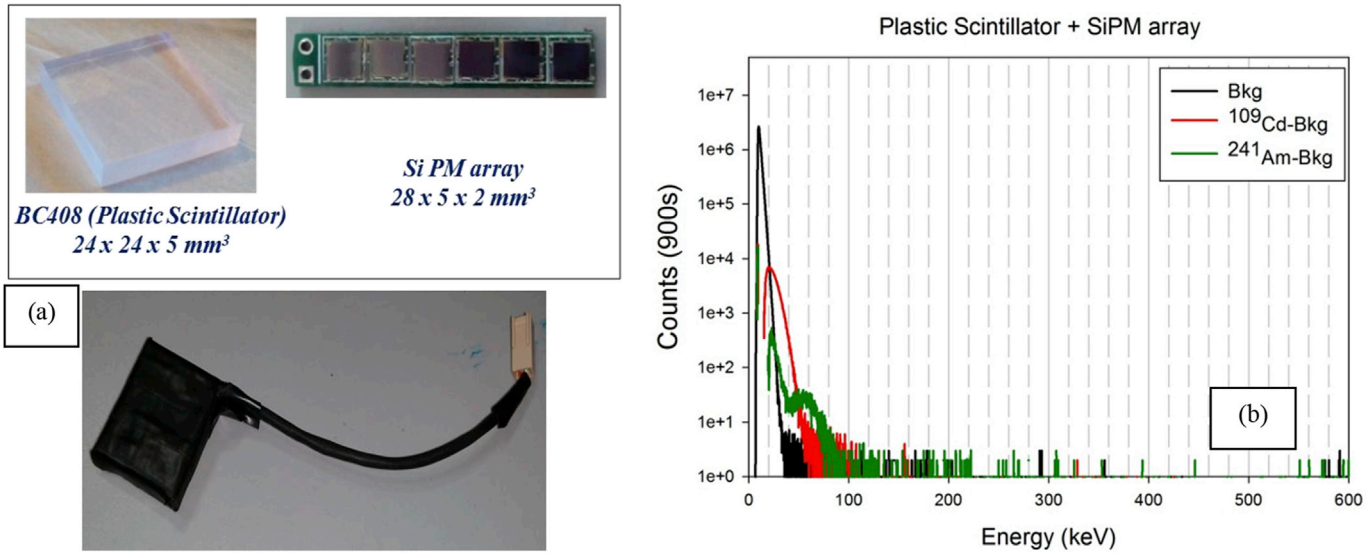

Fig. 17. (a) Plastic scintillator and SiPM array, (b) Energy spectrum for using ^{241}Am and ^{109}Cd source.

4.8. Experimental setup and results for single window Si-PIN detector

The single window Si-PIN detector has been biased to +27 Vdc. The output of the detector is AC coupled to the CSPA. The design of the CSPA for both single window and dual window Si-PIN detectors is identical. The Si PIN detector and the readout electronics are kept inside a light tight box during the experiment to minimize the external stray light effects. A photographic view of the experimental setup is shown in Fig. 18 (a). Fig. 18 (b) is the energy spectrum output obtained using ^{241}Am and ^{109}Cd sources.

Fig. 18 shows that energy threshold obtained is ~10 keV, which is essential for the STEPS subsystem. In all these setups, the testing was

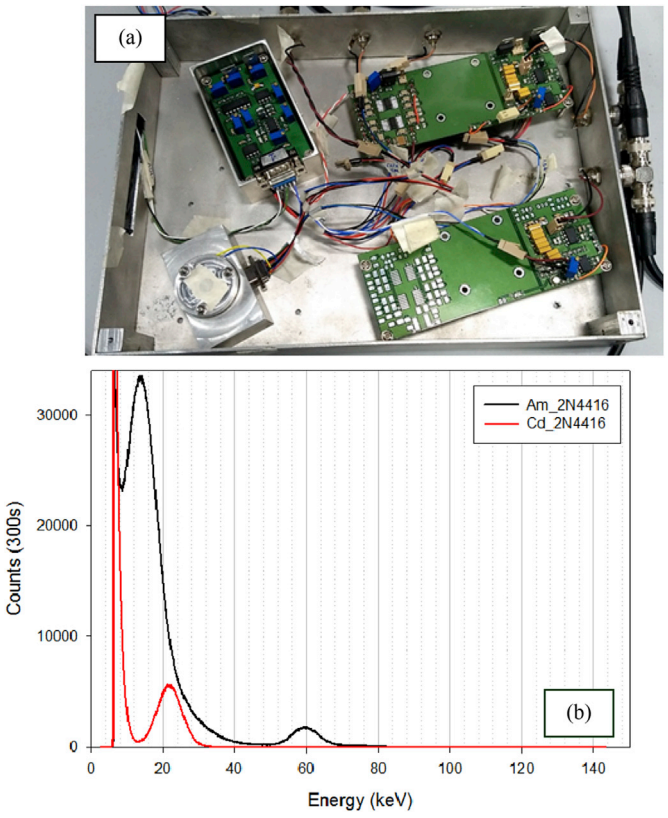

Fig. 18. (a) Single window Si-PIN detector FEE, (b) Energy spectrum output.

carried out for each detector using X-ray sources (^{109}Cd, ^{241}Am).

In the next phase, for the rectangular shaped detector unit, the scintillator detector will be placed below the dual window Si-PIN detector and simultaneous outputs from all three detectors (*viz.* inner window detector, outer window detector and scintillator detector) will be acquired and analyzed. The testing for both types of detector units (rectangular shaped detector units and circular shaped detector units) will be carried out using protons and alpha particles in near future. The performance of the magnet assembly will be evaluated by using electron source (^{90}Sr).

FPGA based processing electronics is used for the ASPEX. The SWIS and the STEPS are having two independent FPGA based processing cards. The power card consisting of relays, relay drivers, DC-DC converters, EMI filters and Low dropout voltage (LDO) regulators is common for both SWIS and STEPS. All these three cards (SWIS FPGA, STEPS FPGA and Power card) are packaged in a single box labeled as ASPEX processing electronics. The processing electronics also has the interface for telemetry and tele-command. The data from the ASPEX processing electronics is transmitted to the base line data handling (BDH) system through low voltage differential signal (LVDS) interface. The design of the data pipeline software is under progress.

The circuits for the SWIS, STEPS and the processing electronics have been designed and tested successfully. The layout design for the PCBs for the engineering model of ASPEX is under progress. The performance of the engineering model will be evaluated inside the thermo-vacuum system. The design for the qualified model and the flight model will be initiated after the performance evaluation of the engineering model.

5. Summary

India's first space-based solar observatory, Aditya-L1, will continuously monitor the Sun with its seven payloads from the L1 vantage point. The ASPEX instrument onboard Aditya-L1 mission has two independent sub-systems *viz.* SWIS and STEPS. The THA-1 of SWIS will work in species differentiated mode and will measure the He^{++} and H^{+} ions separately in 2π radians in the ecliptic plane while THA-2 of SWIS will work in the species integrated mode in 2π radians across the ecliptic plane. The 3 units of the STEPS viz. SR, PS and EP will work in the species differentiated mode and will measure the He^{++} and H^{+} in the Sunward radial, Parker Spiral direction and Earthward directions respectively. The other 3 units of STEPS viz. IM, NP and SP will work in the species integrated mode in the intermediate (in between Sunward radial and Parker Spiral directions) and across the ecliptic plane in the northward and southward directions respectively.

By combining the measurements of solar wind particles from these subsystems in the energy range of 100 eV/n to 20 MeV/n in ecliptic and out of the ecliptic planes from the Sun-Earth L1 Lagrangian point, ASPEX onboard the Aditya-L1 mission will enable to comprehensively address the directional as well as the energy anisotropy of the solar wind particles in the interplanetary medium. Based on the variations of the He^{++}/H^{+} ratio in different directions obtained from the ASPEX measurements, the efficacy of this ratio to mark the arrival of solar (e.g. CME) and interplanetary disturbances (e.g. CIR) at the L1 point will be evaluated. ASPEX measurements will have the potential to throw light on the role of shocks in the generation of energetic particles in the interplanetary medium. Combining ASPEX measurements with the measurements from other payloads, the origin and spatio-temporal distribution of low and high energy solar wind and energetic particles vis-à-vis solar events can be investigated. This in turn, will help in understanding the solar processes and its impact on space weather from the L1 point.

Acknowledgements

We thank Navin Nagrani, Shreya Madhvi, Yash Prajapati, Swati Bhavsar, Rachana Bhatt, Bhargav Malaviya, Anand Dabhi, Arjun Thakor, Vishnu R. Patel, R. Kaila, Pramod and G. P. Ubale for their technical support at various stages of this work. This work at Physical Research Laboratory is supported by the Department of Space, Government of India.

References

Bisoi, Susanta Kumar, Janardhan, P., Chakrabarty, D., Ananthakrishnan, S., Divekar, A., 2014. Changes in quasi-periodic variations of solar photospheric fields: precursor to the deep solar minimum in the cycle 23? Sol. Phys. 289, 41–61. https://doi.org/10.1007/s11207-013-0335-3.

Chotoo, K., Schwadron, N.A., Mason, G.M., Zurbuchen, T.H., Gloeckler, G., Posner, A., Fist, L.A., Galvin, A.B., Hamilton, D.C., Collier, M.R., 2000. The suprathermal seed population for corotating interaction region ions at 1 AU deduced from composition and spectra of H^{+}, He^{++}, and He^{+} observed on wind. J. Geophys. Res. 105, 23107–23122.

Domingo, V., Fleck, B., Poland, A.I., 1995. The SOHO mission: an overview. Space Sci. Rev. 162, 1–37.

Feldman, U., Landi, E., Schwadron, N.A., 2005. On the sources of fast and slow solar wind. J. Geophys. Res. Space Phys. 110.

Feynman, J., Gabriel, S.B., 2000. On space weather consequences and predictions. J. Geophys. Res. 105, 10543–10564.

Fox, N.J., Velli, M.C., Bale, S.D., Decker, R., Driesman, A., Howard, R.A., Kasper, J.C., Kinnison, J., Kusterer, M., Lario, D., Lockwood, M.K., McComas, D.J., Raouafi, N.E., Szabo, A., 2016. The solar Probe plus mission: humanity's first visit to our star. Space Sci. Rev. 204, 7–48.

Goyal, S.K., Shanmugam, M., Patel, A.R., Ladiya, T., Tiwari, Neeraj K., Banerjee, S.B., Vadawale, S.V., Janardhan, P., Chakrabarty, D., Srinivas, A.R., Shukla, P., Kumar, P., Subramanian, K.P., Bapat, B., Adhyaru, P.R., 2016. Multi-directional measurements of high energy particles from the Sun-Earth L1 point with STEPS. Proc. SPIE 9905 (Space Telescopes and Instrumentation).

Isenberg, P.A., 2001. Heating of coronal holes and generation of the solar wind by ion-cyclotron resonance. Space Sci. Rev. 95, 119–131.

Isenberg, P.A., Vasquez Bernard, J., 2007. Preferential perpendicular heating of coronal hole minor ions by the Fermi mechanism. Astrophys. J. 668, 546–556.

Janardhan, P., Bisoi, Susanta K., Gosain, S., 2010. Solar polar fields during cycles 21-23: correlation with meridional flows. Sol. Phys. 267, 267–277.

Janardhan, P., Bisoi, Susanta Kumar, Ananthakrishnan, S., Tokumaru, M., Fujiki, K., 2011. The Prelude to the deep minimum between solar cycles 23 and 24: Interplanetary scintillation signatures in the inner heliosphere. Geophys. Res. Lett. 38, L20108 https://doi.org/10.1029/2011GL049227.

Janardhan, P., Bisoi, Susanta Kumar, Ananthakrishnan, S., Tokumaru, M., Fujiki, K., Jose, L., Sridharan, R., 2015a. A 20 year decline in solar photospheric magnetic

fields: Inner-heliospheric signatures and possible implications. J. Geophys. Res. 120, 5306–5317. https://doi.org/10.1002/2015JA021123.
Janardhan, P., Bisoi, S.K., Ananthakrishnan, S., Sridharan, R., Jose, L., 2015b. Solar and Interplanetary Signatures of a Maunder-like Grand Solar Minimum around the Corner - Implications to Near-Earth Space. Sun Geosphere 10 (2), 147–156.
Janardhan, P., Vadawale, S., Bapat, B., Subramanian, K.P., Chakrabarty, D., Kumar, P., Sarkar, A., Srivastava, N., Satheesh Thambi, R., Vipin Yadav, K., Dhanya, M.B., Nampoothiri, Govin G., Abhishek, J.K., Bhardwaj, A., Subhalakshmi, K., 2017. Probing the heliosphere using in situ payloads on-board Aditya-L1. Curr. Sci. 113, 620–624.
Leinert, C., Pitz, E., Hanner, M., Link, H., 1977. Observations of zodiacal light from HELIOS 1 and 2. J. Geophys.-Z. Geophys. 42, 699–704.
Lemen, James R., Title, Alan M., Akin, David J., Boerner, Paul F., Catherine, Chou, Drake, Jerry F., Duncan, Dexter W., Edwards, Christopher G., Friedlaender, Frank M., Heyman, Gary F., Hurlburt, Neal E., Katz, Noah L., Kushner, Gary D., Michael Levay, Lindgren, Russel W., et al., 2012. The atmospheric imaging assembly (AIA) on the solar dynamics observatory (SDO). Sol. Phys. 275, 17–40.
Leo, W.R., 1994. Techniques for Nuclear and Particle Physics Experiments, second ed. Springer, NewYork.
Muller, D., Marsden, R.G., Cyr, O.C., Gilbert, St, The solar orbiter team, 2013. Solar orbiter. Sol. Phys. 285, 25–70.
Ogilvie, K.W., Desch, M.D., 1997. The WIND spacecraft and its early scientific results. Adv. Space Res. 20, 559–568.
Parker, E.N., 1958. Dynamics of the interplanetary gas and magnetic fields. Astrophys. J. 128, 644–676.
Phillips, J.L., Bame, S.J., Barnes, A., Barraclough, B.L., Feldman, W.C., Goldstein, B.E., Gosling, J.T., Hoogeveen, G.W., McComas, D.J., Neugebauer, M., Suess, S.T., 1995. Ulysses solar wind plasma observations from pole to pole. Geophys. Res. Lett. 22, 3301–3304.
Seetha, S., Megala, S., 2017. Aditya-L1 mission. Curr. Sci. 113, 610–612.
Snyder, C.W., Neugebauer, M., 1964. Interplanetary solar-wind measurements by Mariner II. In: Muller, P. (Ed.), Space Res, vol. 4, pp. 89–113.
Steiger, R., von Richardson, J.D., 2006. ICMEs in the outer heliosphere and at high latitudes: an introduction. Space Sci. Rev. 123, 111–126.
Strong, K., Bruner, M., Tarbell, T., Title, A., Wolfson, C.J., 1994. Trace – the transition region and coronal explorer. Space Sci. Rev. 70, 119–122.
Stone, E.C., Frandsen, A.M., Mewaldt, R.A., Christian, E.R., Margolies, D., Ormes, J.F., Snow, F., 1998. The advanced composition explorer. Space Sci. Rev. 86, 1–22.

Softwares

Agostinelli, S., Allison, J., Amako, K., Apostolakis, J., Araujo, H., Arce, P., Asai, M., Axe, D., Banerjee, S., Barrand, G., Behner, F., Bellagamba, L., Boudreau, J., Brogila, L., Brunengo, A., et al., 2003. GEANT4 – a simulation toolkit. Nucl. Instr. Meth. Res. A 506, 250–303.
COMSOL Multiphysics simulation software, COMSOL Inc.
MATLAB Release 2016, The MathWorks, Inc., Natick, Massachusetts, United States.
Simon, 2008. (R) 8.0 User Manual. Scientific Instrument Services, Inc.